JOURNAL OF MOLECULAR SPECTROSCOPY 94, 38–54 (1982)

Internal Rotation in Methyl Silane by Avoided-Crossing Molecular-Beam Spectroscopy

W. LEO MEERTS

Fysisch Laboratorium, Katholieke Universiteit, Toernooiveld, 6525ED Nijmegen, The Netherlands

AND

IRVING OZIER

Department of Physics, University of British Columbia, 6224 Agriculture Road, Vancouver V6T 2A6, Canada

The avoided-crossing molecular-beam electric-resonance technique was applied to methyl silane in the ground torsional state. A new type of anticrossing is introduced which breaks the torsional symmetry and obeys the selection rules $\Delta J = 0$, $K = +1 \leftrightarrow -1$. For these "barrier" anticrossings, the values of the crossing fields $\mathscr{E}_c$ yield directly the internal rotation splittings; the $\mathscr{E}_c$ are *independent* of the difference $(A-B)$ in the rotational constants. Such anticrossings were observed for J from 1 to 6. Studies were also conducted of several "rotational" anticrossings $(J, K) = (1, \pm 1) \leftrightarrow (2, 0)$ for which $\mathscr{E}_c$ does depend on $(A-B)$. The normal rotational transition $(J, K) = (1, 0) \leftarrow (0, 0)$ was observed in the ground torsional state using the molecular beam spectrometer. The present data on $CH_3{}^{28}SiH_3$ were combined with Hirota's microwave spectra and analyzed with the torsion–rotation Hamiltonian including all quartic centrifugal distortion terms. In addition to evaluating B and several distortion constants, determinations were made of the moment of inertia of the methyl top $I_\alpha = 3.165(5)$ amu-Å^2, the effective rotational constant $A^{\text{eff}} = 56\,189.449(32)$ MHz, and the effective height of the threefold barrier to internal rotation $V_3^{\text{eff}} = 592.3359(73)$ cm^{-1}. The correlations leading to these two effective constants are discussed and the true values of A and V_3 are determined within certain approximations. For the isotopic species $CH_3{}^{30}SiH_3$, barrier and rotational anticrossings were observed. The isotopic changes in A and V_3 were determined, as well as an upper limit to the corresponding change in I_α.

I. INTRODUCTION

Internal rotation has long been a fascinating problem in molecular spectroscopy (*1*, *2*). Although many detailed, high-precision studies have been conducted for the asymmetric rotor, none have been previously carried out for the symmetric top, in spite of the far greater simplicity of its torsion–rotation Hamiltonian $\mathscr{H}_{TR}$. The difficulty lies in the fact that the leading barrier-dependent terms in the energy depend only on quantum numbers which are conserved in electric dipole transitions within the ground vibronic state. These terms therefore do not affect the pure rotational spectrum and cannot be measured by conventional microwave spectroscopy.

To overcome this difficulty, the torsional satellite method was introduced by Kivelson in 1954 (*3*). This technique makes use of the fact that centrifugal distortion

0022-2852/82/070038-17$02.00/0

effects on the leading barrier terms do depend on J and so will affect the normal ($\Delta J = \pm 1$) transition frequencies. With a typical microwave spectrometer, the resulting splittings are too small to be resolved in the ground torsional state, but can be observed in higher torsional levels. The torsional satellite pattern is rather insensitive to the barrier height; furthermore, the analyses to date have depended on the calculation from the structure of the rotational constant about the symmetry axis. Nevertheless, this method is the best of the conventional techniques available for studying symmetric tops and has been applied to many different molecules.

Very recently, an alternative approach (*4*) was introduced based on the avoided-crossing molecular-beam electric-resonance (MBER) method (*5*, *6*). In this technique, two levels with different K are brought to an avoided crossing by an external electric field $\mathscr{E}$. In the anticrossing region, the ($\Delta K = 0$) selection rule is broken; depending on the specific mixing interaction involved, the other selections rules dealing with the conservation of the torsional and nuclear spin parts of the wavefunction can be violated as well. Once the electric dipole moment μ is known, the measurement of the "crossing" field $\mathscr{E}_c$ at which the two levels have their minimum separation can be converted to a determination of the corresponding zero-field splitting Δ_0. Practical difficulties that arise when $\mathscr{E}_c$ becomes large limit such experiments currently to cases where $\Delta_0/\mu \leqslant 5$ GHz/D (*7*). This method of measuring the K dependent terms in $\mathscr{H}_{TR}$ was applied to CH_3CF_3 to determine the rotational constant A, the height V_3 of the threefold barrier to internal rotation, and the moment of inertia I_α of the methyl top (*4*).

In its original form, the avoided-crossing technique was restricted to "rotational" anticrossings in which $|K|$ changed so that Δ_0 contained a large term proportional to $(A-B)$, thereby allowing A to be obtained. However, because of the limit on Δ_0/μ, anticrossings of this type cannot be used to study internal rotation in molecules with large $(A-B)$. As a result, the original method cannot be applied to the very important class of symmetric tops which have only hydrogen (or deuterium) atoms off axis.

In the current work, the anticrossing method was extended in two directions to overcome this limitation and has been applied to CH_3SiH_3. This particular molecule was selected because it has served as the prototype for the torsional satellite method. The older studies of this type (*3*, *8*, *9*) have been greatly extended with new microwave data which will be presented in a later paper (*10*). The two techniques together provide an excellent test both of each other and of the model currently in use for internal rotation.

The first extension of the MBER method consists in demonstrating that anticrossings between different torsional sublevels are allowed satisfying the selection rule $K = +1 \leftrightarrow -1$. In this case, Δ_0 depends only on the difference in the torsional energies; *the leading barrier-dependent terms in a polar symmetric top can be measured regardless of the values of the rotational constants.* Such "barrier" anticrossings have been observed in $CH_3{}^{28}SiH_3$ for $J = 1$ to 6. These measurements, of course, do not allow for a determination of the moment of inertia I_a of the molecule about the symmetry axis.

The second extension of the MBER technique overcomes this difficulty. Although the values of $\mathscr{E}_c$ for the ($\Delta J = 0$, $\Delta|K| \neq 0$) "rotational" anticrossings observed in

CH_3CF_3 are far too high in CH_3SiH_3, such anticrossings with ($\Delta J \neq 0$) can, in principle, occur at much lower fields provided there is a partial cancellation in Δ_0 between the terms involving (A–B) and B. While these have been predicted (*6*), they have not been previously observed. In $CH_3{}^{28}SiH_3$, six different anticrossings of this type have been detected with $(J, K) = (1, \pm 1) \leftrightarrow (2, 0)$, thus providing for a determination of A.

The precision Stark measurements required to calculate the various Δ_0 from the observed $\mathscr{E}_c$ have been described in Paper I (*11*) of this series on methyl silane. All the MBER spectra observed in these two papers were for the ground torsional state.

A thorough analysis was carried out of the anticrossing results and the best existing microwave absorption (*8*) along with the MBER determination in the present work of the frequency of the ($J = 1 \leftarrow 0$) rotational transition. The torsional Hamiltonian $\mathscr{H}_T$ was diagonalized after suitable truncation. Centrifugal distortion effects were taken into account in both overall and internal rotation. In $CH_3{}^{28}SiH_3$, measurements were made of B, I_α, and several distortion constants. Effective values were obtained for A and V_3; the origin of these effective constants and the determination of the true values are discussed. For $CH_3{}^{30}SiH_3$, both barrier and rotational anticrossings were observed; these were used to determine the isotopic changes in A and V_3, as well as to place an upper limit on the corresponding change in I_α.

II. REVIEW OF TORSION-ROTATION THEORY

For a symmetric rotor in the ground vibronic state, the torsion–rotation Hamiltonian $\mathscr{H}_{TR}$ can be written using the internal-axis method (IAM) as (*2*, *8*)

$$\mathscr{H}_{TR} = B\mathbf{J}^2 + (A - B)\mathbf{J}_z^2 + F\mathbf{p}^2 + V(\alpha) + \mathscr{H}_D \,. \tag{1}$$

The first two terms form the Hamiltonian $\mathscr{H}_R$ describing the rigid overall rotation, while the next two form the Hamiltonian $\mathscr{H}_T$ describing the torsional motion. The last term $\mathscr{H}_D$ takes into account various distortion effects. $\mathbf{J}$ is the total angular momentum (exclusive of nuclear spin) and $\mathbf{J}_z$ is its component along the symmetry axis $\hat{z}$. The torsional oscillation is also around the $\hat{z}$ direction in a symmetric rotor; α is the torsional angle between the methyl top and the silyl frame. The quantity $\mathbf{p} = (1/i)(\partial/\partial\alpha)$ is the angular momentum of the internal rotation. For simplicity, the primes used by Lin and Swalen (*2*) have been dropped. The IAM $\mathbf{p}$ is related to the torsional angular momentum in the principal-axis method (PAM) by a simple transformation (*2*)

$$\mathbf{p} \equiv (\mathbf{p})_{IAM} = (\mathbf{p})_{PAM} - \rho\mathbf{J}_z \,; \tag{2}$$

ρ is defined to be that constant which eliminates the coupling term between $\mathbf{J}_z$ and $(\mathbf{p})_{PAM}$ in the PAM torsion–rotation Hamiltonian. If $\mathscr{H}_D \equiv 0$, then

$$\rho \equiv I_\alpha / I_a \,. \tag{3}$$

The rotational constant B is related in the usual way to the moment of inertia I_b about an axis perpendicular to $\hat{z}$. The rotational constant A is similarly related to I_a. The reduced rotational constant

$$F \equiv \hbar^2 I_a/[2I_\alpha(I_a - I_\alpha)]. \tag{4}$$

The potential barrier $V(\alpha)$ to internal rotation can be expanded in a Fourier series

$$V(\alpha) = \sum_{n=1}^{\infty} V_{3n} \frac{1}{2}(1 - \cos 3n\alpha). \tag{5}$$

The expansion coefficients V_{3n} fall off so rapidly with increasing n that only the lower-order terms in the series need be retained.

From the general theory for the interaction between torsion–rotation and vibration (*12*), $\mathscr{H}_D$ can be written to lowest order as[1]

$$\mathscr{H}_D = -D_J\mathbf{J}^4 - D_{JK}\mathbf{J}^2\mathbf{J}_z^2 - D_K\mathbf{J}_z^4 - [D_{Jm}\mathbf{J}^2 + D_{Km}\mathbf{J}_z^2 + D_m\mathbf{p}^2]\mathbf{p}^2$$
$$- [d_J\mathbf{J}^2 + d_K\mathbf{J}_z^2 + d_m\mathbf{p}^2]\mathbf{J}_z\mathbf{p} + \sum_{n=1}^{\infty} \frac{1}{2}(1 - \cos 3n\alpha)[F_{3nJ}\mathbf{J}^2 + F_{3nK}\mathbf{J}_z^2]. \tag{6}$$

The first three terms are present for all symmetric rotors, while the others are particular to systems which undergo internal rotation. The sum on n can be truncated after two or three terms because the series converges very rapidly. The various constants appearing in Eq. (6) are complicated functions of the intramolecular force field (*12*). Here they are treated as fitting parameters to be determined from experiment. Three of these constants were introduced in Kivelson's original work (*3*) and subsequently used by Hirota (*8*). In terms of the older notation, these can be written

$$F_{3J} = 2F_V, \tag{7a}$$

$$D_{Jm} = -G_V, \tag{7b}$$

$$d_J = -L_V. \tag{7c}$$

The subscript V here does not refer to the torsional quantum number.

The eigenvalues E_{TR} of $\mathscr{H}_{TR}$ can be labeled by the quantum numbers $(vJK\sigma m_J)$. The torsional levels are distinguished by $v = 0, 1, 2. \ldots$ The torsional sublevels of symmetry A and E are labeled by $(\sigma = 0)$ and $(\sigma = \pm 1)$, respectively. Each eigenvalue can be classified according to the irreducible representation Γ by which the corresponding torsion–rotation eigenfunction transforms under the operations of the group G_{18} (*13*). An example of the energy level structure and labeling is shown in Fig. 1 for $K = 0$, where $\mathscr{H}_{TR}$ has two distinct eigenvalues, and for $K = 1$, where $\mathscr{H}_{TR}$ has three. The quantum number m_J is the eigenvalue of the component of $\mathbf{J}$ along the space-fixed $\hat{Z}$ axis; the external electric field $\mathscr{E}$, when it is applied, lies along this axis.

To calculate E_{TR}, the distortion term $\mathscr{H}_D$ is treated as a perturbation. The eigenfunctions of the zeroth-order Hamiltonian $\mathscr{H}_0 \equiv \mathscr{H}_R + \mathscr{H}_T$ can be written

$$\psi_\Gamma = |JKm_J> M_{vK\sigma}(\alpha). \tag{8}$$

[1] There are additional terms which should be included in Eq. (6), but these are redundant with the terms already present in $\mathscr{H}_{TR}$. This type of redundancy has been discussed by R. M. Lees and J. G. Baker, *J. Chem. Phys.* **48**, 5299–5318 (1968). These additional terms will be discussed in detail in Ref. (*10*).

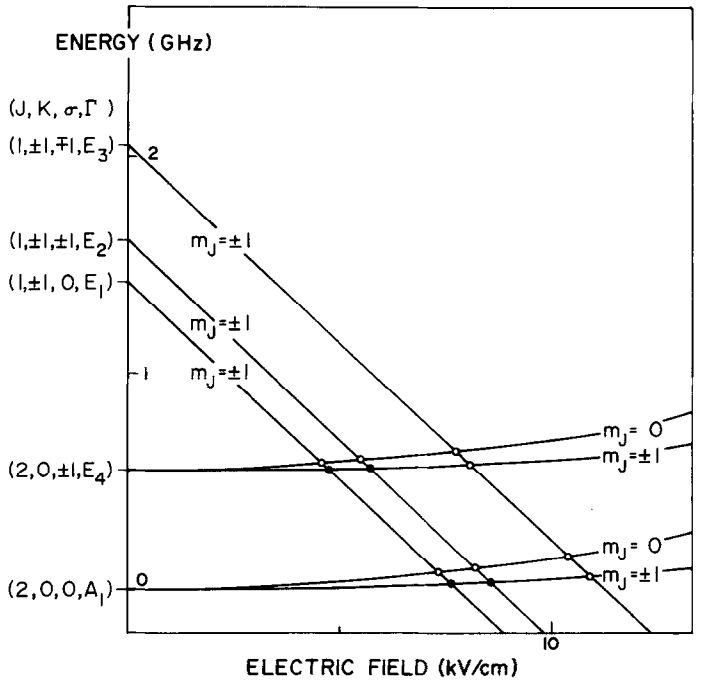

FIG. 1. Schematic plot against the electric field of the energy levels of the $(J, K) = (1, \pm 1)$ and $(2, 0)$ states involved in the rotational anticrossings studied. Upper signs go with upper and lower with lower. For clarity, the quadratic Stark effect of the $(K = 0)$ states has been exaggerated. The nuclear magnetic quantum numbers have been omitted and the hyperfine effects neglected. The repulsion between interacting levels near the avoided crossings is not shown. All 12 anticrossings were detected, but precision measurements of the crossing fields were made only for those indicated by heavy dots.

Because there is no coupling between overall and internal rotation, the problem is separable. The symmetric top functions $|JKm_J\rangle$ diagonalize $\mathscr{H}_R$. The torsional functions $M_{vK\sigma}$ diagonalize $\mathscr{H}_T$. These can be expanded in a Fourier series (*2*)

$$M_{vK\sigma}(\alpha) = \sum_{k=-\infty}^{\infty} A_{3k+\sigma}^{vK} \mathbf{Z}_{3k+\sigma}^{K}, \tag{9}$$

where

$$\mathbf{Z}_{3k+\sigma}^{K} = \frac{1}{(2\pi)^{1/2}} \exp[i\alpha(3k + \sigma - \rho K)]. \tag{10}$$

The expansion coefficients $A_{3k+\sigma}^{vK}$ and the unperturbed energy $E_T^{(0)}$ are calculated by diagonalizing for each (K, σ) the matrix for $\mathscr{H}_T$ set up in the $\mathbf{Z}$ representation. This matrix is truncated in k after enough terms are included that the energy obtained is sufficiently accurate for the highest v of interest.

The effect of $\mathscr{H}_D$ is then treated with first-order perturbation theory. This term is diagonal in J, K, m_J, and σ, but has matrix elements off-diagonal in v. To test whether the higher-order perturbations are important, the matrix for $(\mathscr{H}_T + \mathscr{H}_D)$ was diagonalized for each (v, J, K, σ) using representation (*8*). For the low J values studied here, the difference between the two calculations was negligible.

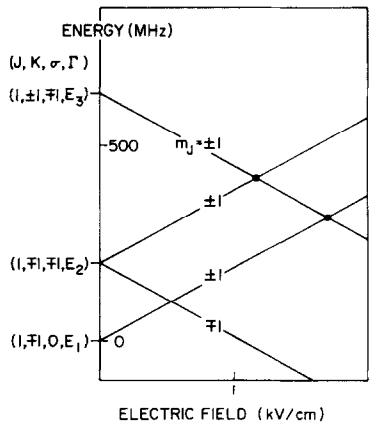

FIG. 2. Schematic plot against electric field of the energy levels for the $(K, \sigma) = (\pm 1, \mp 1)$, $(\mp 1, \mp 1)$, and $(\mp 1, 0)$ states with $J = 1$ involved in the barrier anticrossings studied. The two heavy dots indicate the avoided crossings for which precision measurements of the crossing field have been made. With one exception, upper signs go with upper and lower signs with lower. If the third intersection were an avoided crossing with the same characteristics as the other two, then the third case would be the exception: upper signs would go with lower and vice versa. However, this third intersection seems to be a true crossing since no anticrossing transitions could be detected.

III. EXPERIMENTAL DETAILS

The experimental methods and conditions used for the anticrossing measurements were very similar to those in the Stark experiments on methyl silane in Paper I[2] and those in the earlier avoided-crossing studies (*6*, *7*). The basic MBER apparatus used has been described in detail elsewhere (*14*). The source conditions for the seeded nozzle beam were the same as those used in Paper I to study the low K Stark transitions. The pyrex plates of the C field (*7*) were coated in the parallel plate configuration, which gives better homogeneity, but permits only transitions with $\Delta m_T = 0$, where m_T is the eigenvalue of the component of the total angular momentum along $\hat{\mathcal{E}}$. The transition region was 30 mm long, giving a time-of-flight linewidth $\Delta\nu_T \sim 15$ kHz and field inhomogeneities $\sim$20 ppm. For each isotopic species, the mass-to-charge setting of the detector was the same as that for the Stark studies in Paper I. The techniques employed to calibrate the electric field and to measure the crossing fields have been discussed in detail elsewhere (*6*, *7*).

For the $(J = 1 \leftarrow 0)$ rotational transition at 22 GHz, the C field was similar to that described by Dijkerman *et al.* (*15*). It consisted of a parallel plate system in combination with a microwave horn. In the frequency range 12 to 40 GHz, symmetric lineshapes are obtained with a full-width at half-maximum of 13 kHz.

IV. DETERMINATION OF THE ZERO-FIELD SPLITTINGS

1. The Barrier Anticrossings

From the energy level diagram in Fig. 2 showing the torsional splittings and Stark effect for $|K| = 1$, $|m_J| = 1$, it was initially anticipated that three different

[2] Paper 1 refers to Ref. (*11*).

anticrossing systems could be studied. Only two of these proved to be observable. In both of these, the level (α) of higher energy in zero field has $\Gamma = E_3$. When the level (β) of lower energy has $\Gamma = E_2$, both levels are of E torsional symmetry; this is called an EE anticrossing and $\Delta_0 \equiv \nu_{EE}$. When level (β) has $\Gamma = E_1$, one of the interacting levels has E torsional symmetry and the other has A; this is called an EA anticrossing and $\Delta_0 \equiv \nu_{EA}$. In spite of several careful attempts, the second EA anticrossing between upper level ($\Gamma = E_2$) and lower level ($\Gamma = E_1$) was not detected. Since this same behavior occurred for CH_3SiF_3 (*16*), it has been tentatively concluded that mixing between ($\Gamma = E_2$) and ($\Gamma = E_1$) is forbidden by symmetry.

Careful consideration must be given to the selection rules for all the quantum numbers of the interacting levels. Each anticrossing system involves many levels because of the "sign-doubling" (*6*) shown in Fig. 2 and the nuclear spin magnetic quantum numbers m_H^T and m_H^F for the top and frame total proton spins, respectively. For each system in Fig. 2, there were initially three possible assignments. One consists of a series of separable two-level interactions in which $\Delta K = \pm 2$, $\Delta m_J = 0$, $\Delta m_H^T = \Delta m_H^F = 0$. The second consists of a similar series in which $\Delta K = 0$, $\Delta m_J = \pm 2$, $\Delta(m_H^T + m_H^F) = \mp 2$. The third consists of a series of separable multilevel interactions formed from a hybrid of the first two. When a magnetic field was applied the frequency and intensity did not change. This eliminates the second assignment, since such a spectrum would split into two lines, each moving with an effective g factor g_{eff} approximately twice the proton g factor g_H (see Eq. (19) of Ref. (*6*)). Furthermore, no satellite lines were observed; this eliminates the third assignment as can be seen from the discussion of Fig. 2 in Ref. (*6*).

To investigate the selection rules further, attempts were made to observe a variety of other barrier anticrossings. It was firmly established that such avoided crossings with $\Delta|K| = 0$ occur only for $|K| = 1$. This is not surprising, since otherwise the mixing would require an interaction of rather high tensor rank. The many anticrossings searched for with $|K| = 1$ are listed in Table I. Although the changes in m_J could be easily established from the second-order Stark effect and/or the effect of an external magnetic field, in many cases the changes in m_H^T and m_H^F could not be uniquely determined because the nuclear g factors for the top and frame are equal. The selection rules deduced can be summarized as (J, K, σ, Γ) = (J, ± 1, ∓ 1, E_3) $\leftrightarrow$ (J, ∓ 1, ∓ 1, E_2) for the EE anticrossing and (J, ± 1, ∓ 1, E_3) $\leftrightarrow$ (J, ∓ 1, 0, E_1) for the EA anticrossing, with $\Delta m_J = 0, \pm 1, \mp 1, \pm 2, \mp 2$ for both types. Unless otherwise specified, it can be assumed throughout that upper signs go only with upper and lower only with lower.

From these selection rules, it is clear that the mixing matrix element η arises from nuclear hyperfine interactions. A complete understanding of this mixing requires a full study of the hyperfine Hamiltonian for a molecule of G_{18} symmetry, similar to that done earlier for C_{3v} symmetry (*6*). Such a study is currently underway. However, the preliminary conclusion can be drawn that, since Δm_J can equal ± 2, the spin–spin interaction $\mathscr{H}_{II}$ provides at least part of the mixing when $\Delta m_J = 0$. There is strong evidence that $\mathscr{H}_{II}$, in fact, dominates the ($\Delta m_J = 0$) mixing. The EA and EE ($\Delta m_J = 0$) anticrossings for ($J = 3$, $m_J = \pm 2$) were unobservable, in spite of the fact that similar signals were detected for many other (J, m_J) values. Since the factor $[3m_J^2 - J(J + 1)]$ occurs in the η with $\Delta m_J = 0$

TABLE I

Summary of the Selection Rules Investigated for Barrier Anticrossings in CH_3SiH_3

J	Upper State α K = ±1			Lower State β K' = ±1			Δm_J	Label	Remarks
	σ	Γ	m_J	σ'	Γ'	m'_J			
1,2,3,5,6	$\overline{+}1$	E_3	$\pm J^a$	0	E_1	$\pm J^a$	0	EA	
2	$\overline{+}1$	E_3	± 1	0	E_1	± 1	0	EA	
3	$\overline{+}1$	E_3	± 2	0	E_1	± 2	0	EA	not observed
1	$\overline{+}1$	E_3	0	0	E_1	± 1	± 1	EA	
2,3	$\overline{+}1$	E_3	0	0	E_1	± 2	$\overline{+}2$	EA	
3	$\overline{+}1$	E_3	± 1	0	E_1	± 3	$\overline{+}2$	EA	
2	$\overline{+}1$	E_3	± 2	0	E_1	0	± 2	EA	
3	$\overline{+}1$	E_3	± 3	0	E_1	± 1	± 2	EA	
1,2,3,5	$\overline{+}1$	E_3	$\pm J^a$	$\overline{+}1$	E_2	$\pm J^a$	0	EE	
2	$\overline{+}1$	E_3	± 1	$\overline{+}1$	E_2	± 1	0	EE	
3	$\overline{+}1$	E_3	± 2	$\overline{+}1$	E_2	± 2	0	EE	not observed
2	$\overline{+}1$	E_3	0	$\overline{+}1$	E_2	± 1	$\overline{+}1$	EE	
4	$\overline{+}1$	E_3	± 2	$\overline{+}1$	E_2	± 1	± 1	EE	
1,2	± 1	E_2	$\pm J^a$	0	E_1	$\pm J^a$	0	EA	not observed

a - The labelling means $m_J = m'_J = \pm J$ for the J-values in the first column.

for all spin–spin interactions and this factor vanishes for ($J = 3$, $m_J = \pm 2$), $\mathscr{H}_{II}$ seems to provide the mixing mechanism for the barrier anticrossings.

The particular anticrossings with ($\Delta m_J = 0$) are very unusual in that, aside from the change in σ, the only difference between the interacting levels is in the *sign* of K. Thus, except possibly for very small σ-dependent effects, the upper level (α) and the lower level (β) have the same second-order Stark effect, the same diagonal hyperfine matrix elements, and the same Zeeman effect. This means that the crossing field $\mathscr{E}_c$ is independent of the effective anisotropy $(\alpha_\parallel - \alpha_\perp)_{eff}$ in the polarizability (see Paper I), the nuclear hyperfine constants, and the g factors. The value of Δ_0 depends only on the torsional splitting and the effective dipole moment $\mu_Q(J, K)$ defined in Eq. (1) of Paper I. These anticrossings are therefore ideally suited to precision studies of the barrier parameters.

Although this precision requires the full analysis described in Section II, considerable insight into the problem can be obtained from a much simpler treatment.

The value of $\mathscr{H}_D$ is neglected. The torsional energy $E_T^{(0)}$ is represented by a Fourier expansion (*2*)

$$E_T^{(0)}(vK\sigma) = \sum_{n=0}^{\infty} a_n(v)F \cos\left[\frac{2n\pi}{3}(\rho K - \sigma)\right], \tag{11}$$

where the expansion coefficients $a_n(v)$ are functions only of the reduced barrier height $s \equiv 4V_3/9F$, which equals 32 for methyl silane. For the ground torsional state, the case of interest here, $|a_1/a_2| \gtrsim 3000$ and only the first term is retained.

In this approximation,

$$\nu_{EE} = -a_1 F 3^{1/2} \sin(2\pi\rho/3); \tag{12a}$$

$$\nu_{EA} = -a_1 F[(3/2)\cos(2\pi\rho/3) + (3^{1/2}/2)\sin(2\pi\rho/3)]. \tag{12b}$$

These equations can be represented by a triangle whose sides are ν_{EE}, ν_{EA}, and $(3/2)|a_1F|$. Angle $(\pi/3)$ is opposite $(3/2)|a_1F|$ and angle $(2\pi\rho/3)$ opposite ν_{EE}. Equations (12) can be easily inverted:

$$\tan(2\pi\rho/3) = (3^{1/2}/2)\nu_{EE}/[\nu_{EA} - (\nu_{EE}/2)], \tag{13a}$$

$$|a_1F| = (2/3)[\nu_{EA}^2 + \nu_{EE}^2 - \nu_{EA}\nu_{EE}]^{1/2}. \tag{13b}$$

These equations show that, for each J, the parameters ρ and $|a_1F|$ can be determined independently. If A is known, then ρ will give I_α, while A, ρ, and a_1F will give V_3. Further, it is important to note that ρ depends only on a *ratio* of zero-field splittings. Since the measured values of ν_{EE} and ν_{EA} depend to excellent approximation only on the linear Stark effect for $(\Delta m_J = 0)$ anticrossings, ρ is independent of the dipole moment $\mu_Q(J, K)$ involved.

The crossing field $\mathscr{E}_c$ was measured for each of the barrier anticrossings listed in Table II. The J values ranged from 1 to 6. The $\mathscr{E}_c$ fell between ~1700 and ~6000 V/cm for the EA cases and between ~1200 and ~3600 V/cm for the EE cases studied. The full-width $\Delta\nu_{obs}$ at half-maximum observed for all transitions was ~20 kHz. For $1 \leq J \leq 3$, the signal-to-noise ratio on a single sweep with a time constant of 1 sec varied from 7 to 30. A signal averager was used for the weaker of these lines as well as for the $(J = 5)$ and $(J = 6)$ transitions.

To obtain each Δ_0 from its $\mathscr{E}_c$, the computer program developed for the Stark study in Paper I was used to calculate the frequency (i.e., Δ_0) and error for the corresponding forbidden transition. The error obtained in this way takes proper account of all of the correlations among the Stark parameters. This dipole error was then combined in quadrature with two others: the frequency error from determining center of the anticrossing lines and the calibration error of 20 ppm (*6*) from the long-term stability of the voltage source. For these absolute measurements, the total uncertainty was dominated by the calibration term with a small contribution from the dipole term; the frequency error was negligible. Each measured Δ_0 and its error are given in Table II.

For properly chosen cases, the accuracy in the difference between two distinct Δ_0 can be improved considerably by observing both anticrossings in the same electric

TABLE II

Energy Splittings Δ_0 in MHz of $CH_3{}^{28}SiH_3$ from Anticrossing and Microwave Experiments

v	Upper State J	K	σ	Γ	Lower State J'	K'	σ'	Γ'	Observed Splitting	Observed-Calculated	Label
0	1	±1	±1	E_2	2	0	0	A_1	1 623.282 (33)	-0.009	$\nu_{\pm1,0}$
0	1	±1	0	E_1	2	0	0	A_1	1 424.729 (29)	0.007	$\nu_{0,0}$
0	1	±1	±1	E_2	2	0	±1	E_4	1 059.961 (22)	0.001	$\nu_{\pm1,\pm1}$
0	1	±1	0	E_1	2	0	±1	E_4	861.392 (18)	-0.000	$\nu_{0,\pm1}$
0	1	±1	∓1	E_3	1	∓1	0	E_1	635.637 (13)	-0.015	ν_{EA}
0	2	±1	∓1	E_3	2	∓1	0	E_1	635.704 (13)	-0.002	ν_{EA}
0	3	±1	∓1	E_3	3	∓1	0	E_1	635.792 (13)	0.004	ν_{EA}
0	5	±1	∓1	E_3	5	∓1	0	E_1	636.037 (14)	0.004	ν_{EA}
0	6	±1	∓1	E_3	6	∓1	0	E_1	636.211 (16)	0.015	ν_{EA}
0	ν_{EA} (J = 2) - ν_{EA} (J = 5)								-0.3276 (80)	-0.0007	Relative
0	1	±1	∓1	E_3	1	∓1	∓1	E_2	437.083 (9)	0.000	ν_{EE}
0	2	±1	∓1	E_3	2	∓1	∓1	E_2	437.114 (9)	-0.005	ν_{EE}
0	3	±1	∓1	E_3	3	∓1	∓1	E_2	437.173 (9)	0.000	ν_{EE}
0	5	±1	∓1	E_3	5	∓1	∓1	E_2	437.340 (9)	0.005	ν_{EE}
0	ν_{EE}(J = 2) - ν_{EE}(J = 5)								-0.2199 (50)	-0.0043	Relative
0	1	0	0	A_2	0	0	0	A_1	21 937.885 (10)	-0.001	1 ← 0
0	1	0	±1	E_4	0	0	±1	E_4	21 937.913 (10)	0.003	1 ← 0
1	1	0	0	A_2	0	0	0	A_1	21 873.10	0.076	1 ← 0 [a]
1	1	0	±1	E_4	0	0	±1	E_4	21 872.46	0.111	1 ← 0 [a]
2	1	0	0	A_2	0	0	0	A_1	21 808.85	0.018	1 ← 0 [a]
2	1	0	±1	E_4	0	0	±1	E_4	21 814.41	0.057	1 ← 0 [a]
0	2	±1	0	E_1	1	±1	0	E_1	43 875.28[b]	-0.061	2 ← 1 [a]
0	2	±1	±1	E_2	1	±1	±1	E_2	43 875.28[b]	-0.079	2 ← 1 [a]
0	2	±1	∓1	E_3	1	±1	∓1	E_3	43 875.28[b]	-0.115	2 ← 1 [a]
1	2	±1	0	E_1	1	±1	0	E_1	43 745.41	0.016	2 ← 1 [a]
1	2	±1	±1	E_2	1	±1	±1	E_2	43 744.75	-0.108	2 ← 1 [a]
1	2	±1	∓1	E_3	1	±1	∓1	E_3	43 743.88	0.004	2 ← 1 [a]
2	2	±1	0	E_1	1	±1	0	E_1	43 618.53	0.030	2 ← 1 [a]
2	2	±1	±1	E_2	1	±1	±1	E_2	43 622.73	0.014	2 ← 1 [a]
2	2	±1	∓1	E_3	1	±1	∓1	E_3	43 632.89	-0.083	2 ← 1 [a]

a - These frequencies were taken from Ref. (8). The errors used in the fit were 100 kHz. All other data are from the present investigation.
b - This triplet was not resolved. In the fit, we used the average of the three, weighted by the relative intensities.

field (*6*). In this way, the *EA* and *EE* zero-field splittings were determined for (J = 2) relative to those for (J = 5) from the avoided crossings (J, K, m_J) = (2, ±1, ±1) ↔ (2, ∓1, ±1) and (5, ±1, ±5) ↔ (5, ∓1, ±5). The calibration error was reduced to a negligible 2 ppm arising from the short-term stability of the voltage source. The total error now is dominated by the dipole term with a small contribution from the frequency term. The results are presented in Table II.

2. *The Rotational Anticrossings*

For an accurate determination of A, the observation of an anticrossing with $\Delta|K| \neq 0$ is required. Because of an almost complete cancellation in Δ_0 between the term in $(A-B)$ and that in B, the pure rotational contribution to the zero-field splitting for the avoided crossing between $(J, K) = (1, \pm 1)$ and $(2, 0)$ is only ~ 1.3 GHz. The energy level scheme for this "rotational" anticrossing is illustrated in Fig. 1. Because of the focusing requirements for detecting the anticrossing signals (*6*), only the anticrossings involving a focused lower state (β) can be observed, so that the (2, 0) levels involved can have $m_J = 0$ or ± 1, but not ± 2. Because of the torsional splittings, there are 12 possible anticrossings of this type, six with $\Delta|m_J| = 0$ and six with $\Delta m_J = \pm 1$. Since $\Delta K = \pm 1$, the symmetry breaking terms in the total Hamiltonian that mix the anticrossing levels must arise from the nuclear hyperfine interactions (*6*). All 12 anticrossings were detected.

The four strongest avoided crossings with $\Delta|m_J| = 0$ were selected for accurate measurement of their crossing fields. For each one, the zero-field splitting Δ_0 has been assigned a specific label $\nu_{\sigma,\sigma'}$. In order of decreasing magnitude, these are $\nu_{\pm 1,0}$ for $(J, K, \sigma) = (1, \pm 1, \pm 1) \leftrightarrow (2, 0, 0)$; $\nu_{0,0}$ for $(1, \pm 1, 0) \leftrightarrow (2, 0, 0)$; $\nu_{\pm 1,\pm 1}$ for $(1, \pm 1, \pm 1) \leftrightarrow (2, 0, \pm 1)$; $\nu_{0,\pm 1}$ for $(1, \pm 1, 0) \leftrightarrow (2, 0, \pm 1)$. The anticrossing transitions were observed with signal-to-noise ratios between 2 and 6 for a single sweep with a time constant of 2 sec. The actual measurements were again taken with a signal averager. The observed linewidth $\Delta\nu_{obs}$ was ~ 28 kHz arising from an inhomogeneity contribution to ~ 24 kHz and a time-of-flight contribution of ~ 15 kHz.

The values of the Δ_0 and their errors were calculated with the same procedures as were used for the barrier anticrossings in Section IV.1. The results are given in Table II. In this case, the calibration error ranging from 17 to 32 kHz was dominant. Although the rotational anticrossings can have a frequency shift due to the nuclear hyperfine interactions, this effect is a few kilohertz at most and is insignificant compared to the calibration error.

The internal consistency of the data can be demonstrated by comparing various combination differences. From Table II, $(\nu_{0,0} - \nu_{0,\pm 1}) = 563.337$ MHz and $(\nu_{\pm 1,0} - \nu_{\pm 1,\pm 1}) = 563.321$ MHz. From Fig. 1, these should be equal, as indeed they are to well within the experimental error. Furthermore, from Table II, $(\nu_{\pm 1,\pm 1} - \nu_{0,\pm 1}) = 198.569$ MHz; $(\nu_{\pm 1,0} - \nu_{0,0}) = 198.553$ MHz; and, for $(J = 1)$, $(\nu_{EA} - \nu_{EE}) = 198.554$ MHz. Again, these differences should be equal and do agree to well within the error.

3. *The Isotopic Species $CH_3{}^{30}SiH_3$*

Valuable insight into the internal rotation problem can be obtained from isotopic effects. For $CH_3{}^{30}SiH_3$ in natural abundance, measurements were made of three different $(\Delta m_J = 0)$ barrier anticrossings. In each case, the isotopic shift in $\mathcal{E}_c$ corresponds to a frequency difference of only a few hundred kilohertz. This made it possible to measure $\mathcal{E}_c$ for $CH_3{}^{30}SiH_3$ *relative* to $\mathcal{E}_c$ for $CH_3{}^{28}SiH_3$, thus considerably improving the accuracy in the difference (*6*). By using the isotopic change in $\mu_Q(J = 1, K = 1)$ measured in Paper I, the absolute values of $\Delta_0(30)$ and the

TABLE III

Energy Splittings for $CH_3{}^{30}SiH_3$ and Isotopic Shifts Relative to $CH_3{}^{28}SiH_3$

Upper State J K σ Γ	Lower State J' K' σ' Γ'	Label	Observed Splitting Δ_o (MHz)	$\Delta_o(30) - \Delta_o(28)$
1 ±1 0 E_1	2 0 0 A_1	$\nu_{0,0}$	2 235.789 (45)	
1 ±1 ∓1 E_3	1 ∓1 0 E_1	ν_{EA}	635.102 (13)	-534.7 (2.8)[a]
2 ±1 ∓1 E_3	2 ∓1 0 E_1	ν_{EA}	635.169 (13)	-534.7 (2.8)
1 ±1 ∓1 E_3	1 ∓1 ∓1 E_2	ν_{EE}	436.724 (9)	-359.2 (3.3)[a]

a - These measurements were used in calculating the isotopic change in ρ.

shifts $[\Delta_0(30) - \Delta_0(28)]$ were determined. The results are listed in Table III. The error in the absolute numbers is dominated by the calibration error, while that in the differences contains comparable contributions from the short-term stability of the voltage source, the uncertainty in the isotopic change in μ, and the frequency errors.

The value of $\mathscr{E}_c$ was also determined for the $\nu_{0,0}$ rotational anticrossing in $CH_3{}^{30}SiH_3$ with $\Delta|m_J| = 0$. Because of the relatively large isotopic change in B, the corresponding $\mathscr{E}_c$ in the parent species was lower by a factor ~ 1.6, so that relative measurements were not possible. The result obtained for $\nu_{0,0}$ is given in Table III.

4. *The Rotational Transitions*

The frequencies for allowed pure rotational transitions obeying the normal selection rules $\Delta J = \pm 1$, $\Delta(\sigma K) = 0$ are given by (see Section II)

$$\nu(v, J, K, \sigma) = 2(J+1)\left\{B + \sum_{n=1}^{\infty} F_{3nJ}\left\langle \frac{1}{2}(1 - \cos 3n\alpha)\right\rangle_{vK\sigma} - D_{Jm}\langle \mathbf{p}^2\rangle_{vK\sigma} - d_J K\langle \mathbf{p}\rangle_{vK\sigma}\right\} - 2(J+1)K^2 D_{JK} - 4(J+1)^3 D_J . \quad (14)$$

As usual, only the lower-order terms on the sum on n need be retained. The quantity in curly brackets in Eq. (14) is the effective B value B_{eff} that is the basis of the torsional satellite method (*3*, *12*, *8*). The angular brackets $\langle\ \rangle_{vK\sigma}$ represent diagonal matrix elements in the torsional state $|vK\sigma\rangle$.

For $CH_3{}^{28}SiH_3$, Hirota (*8*) gives frequencies for such transitions for $v \leq 4$ with $(J, K) = (1, 0) \leftarrow (0, 0)$ and with $(2, \pm 1) \leftarrow (1, \pm 1)$. With one exception, the frequencies with $v \leq 2$ are listed in Table II. The lines with $v \geq 3$ are discussed in Section VI. No errors are quoted because none are specified in the original work. It was assumed that the experimental uncertainties were 100 kHz.

The exception mentioned above is the line with $(1, 0) \leftarrow (0, 0)$ for the torsional ground state. From Eq. (14), this line consists of two components at frequencies

$\nu(0, 0, 0, 0)$ and $\nu(0, 0, 0, \pm 1)$. This spectrum was remeasured with the MBER spectrometer in an attempt to resolve the doublet splitting of 24 kHz expected from a preliminary analysis. The instrumental linewidth was 13 kHz and a signal-to-noise ratio of 100 was attained for a single sweep with a time constant of 1 sec. A partial resolution of the splitting was achieved. However, because of small hyperfine effects, there was considerable uncertainty in determining the two "hyperfine-free" frequencies $\nu(0, 0, 0, 0)$ and $\nu(0, 0, 0, \pm 1)$. To allow for these effects, each frequency was assigned an error of 10 kHz. The results are given in Table II. They agree well with Hirota's value for the unresolved pair.

An attempt was made also to observe this doublet for $v = 1$. With the standard source conditions used for the anticrossings, these lines could not be detected, indicating that the torsional temperature is lowered considerably in the nozzle. The source conditions were varied, but we were unable to observe the transitions.

V. THE ABSOLUTE SIGNS OF THE ROTATIONAL g FACTORS

In Paper I, the conventional MBER spectrum was used to determine the magnitudes of the two rotational g factors $g_\perp$ and $g_\parallel$ as well as showing that the relative sign is positive. The absolute signs were established here by a method developed earlier (*6*) based on studying an anticrossing with ($\Delta m_J \neq 0$) in a magnetic field. For this purpose, the EA barrier avoided crossing $(J, K, \sigma, \Gamma, m_J) = (1, \pm 1, \mp 1, E_3, 0) \leftrightarrow (1, \mp 1, 0, E_1, \pm 1)$ was observed in a magnetic field of 0.4 T. The spectrum was found to consist of two magnetic components, whose effective g factors were

$$g_{\text{eff}} = \mp[g_{\text{H}} - \tfrac{1}{2}(g_\perp + g_\parallel)]. \tag{15}$$

The hydrogen shielding effects are negligible. It was found that $|g_{\text{eff}}| = 5.65686(17)$ nm. From the known value for the hydrogen g factor g_{H} (*17*), it follows that $(g_\perp + g_\parallel) = -0.1426(7)$ nm. Thus both g factors are negative. From the results in Paper I, it was found that $|g_\perp + g_\parallel| = 0.14306(13)$ nm. The two magnitudes agree well; this comparison provides a strong test of the data. The significance of this sign determination is discussed in Paper I.

VI. ANALYSIS AND DISCUSSION

A least-squares analysis of the data for $CH_3{}^{28}SiH_3$ in Table II was carried out using the procedure outlined in Section II. There is clearly not enough information to determine all the constants in Eqs. (1) and (6). The first step in overcoming this problem was to fix D_J and D_{JK} at values from the mm-wave spectrum (*10*).

Because of the many correlations, it was necessary to introduce three effective parameters. Four of the constants which enter only in K-independent terms are highly correlated: A, D_K, D_{Km}, and F_{3K}. These are sensitive only to the beam data. Because A and D_K cannot be separated, D_K was fixed at the force-field value (*18*). Two linear combinations of the remaining three constants were determined, A^{eff} and D_{Km}^{eff}:

$$A^{\text{eff}} = A - D_{Km}\overline{\langle \mathbf{p}^2 \rangle_0} + F_{3K}\overline{\langle (1/2)(1 - \cos 3\alpha) \rangle_0}, \tag{16a}$$

$$D_{Km}^{\text{eff}} = D_{Km} + \lambda F_{3K}; \tag{16b}$$

TABLE IV

Molecular Constants for Methyl Silane

		$CH_3{}^{28}SiH_3$	$CH_3{}^{30}SiH_3$
A^{eff}	(MHz)	56 189.449 (32)	56 190.276 (52)
B	(MHz)	10 986.378 (22)	10 824.315[a]
D_J	(kHz)	10.71 [a]	10.71 [c]
D_{JK}	(kHz)	45.59 [a]	45.59 [c]
D_K	(kHz)	189.65 [b]	189.65 [c]
ρ		0.351 8127 (49)	0.351 8197 (91)
V_3^{eff}	(cm^{-1})	592.3359 (73)	592.4420 (84)
F_{3J}	(MHz)	-138.27 (17)	-138.27 [c]
F_{9J}	(MHz)	-2.653 (65)	-2.653 [c]
D_{Jm}	(MHz)	0.7071 (41)	0.7071[c]
D_{Km}^{eff}	(MHz)	10.6 (2.0)	10.6 [c]
d_J	(MHz)	-0.157 (29)	-0.157 [c]

a - This is fixed at the value taken from Ref. (10).
b - This is fixed at the force-field value. (18)
c - This is fixed at the corresponding value for $CH_3{}^{28}SiH_3$.

$\overline{\langle\Omega\rangle_0}$ is the unweighted average over σ of the diagonal matrix elements of operator Ω for $v = 0$ and any fixed K. The particular value of K selected to calculate this mean need not be specified because the average is independent of K for $v = 0$ to an accuracy much higher than necessary here (*10*). The calculated value of the numerical constant λ is 0.0115; it is a function only of the reduced barrier height s. The origin of these effective parameters will be discussed elsewhere (*10*). Because V_3 is related to A through s, the use of A_{eff} necessitated the introduction of

$$V_3^{eff} = (9/4)sA^{eff}/[\rho(1-\rho)]. \tag{16c}$$

The determinable parameters[3] are listed in Table IV, along with the best fit values. Table II lists the differences between the observed frequencies and those calculated from these constants. The agreement is excellent. The value of D_{Km}^{eff} is determined to only 20%, but it is required to remove systematic deviations of about 150 kHz for the rotational anticrossing data. The constants in Eqs. (5) and (6) but omitted from Table IV were fixed at zero; they either did not improve the fit or were undeterminable.

[3] F is not treated as an independent parameter, but is set equal to $A_{eff}/\rho(1-\rho)$. Strictly speaking, this step and other small effects discussed in Ref. (*10*) require the addition of a term $\zeta\mathbf{p}^2$ to $\mathscr{H}_{TR}$, where ζ is an empirical torsion distortion constant. However, ζ could not be determined in the fit and was fixed at zero.

TABLE V

Values Obtained for True Parameters under Different Assumptions

	Assume $F_{3K} \equiv 0$	Assume $D_{Km} \equiv 0$
A (MHz)	56 251.	56 106.
V_3 (cm^{-1})	593.12	591.27
D_{Km} (MHz)	10.7	0
F_{3K} (MHz)	0	944.

The constant F_{9J} was included in this best model, while we omitted F_{6J}, which was initially expected to be much larger. The constant F_{9J} was chosen because it reduced the χ^2 to 8.7 while F_{6J} gave a χ^2 of 14.7. The reduction is significant in an F test at the 85% level, but, perhaps more important, the change in the χ^2 arose almost entirely from the two relative measurements in the beam data. The fit with F_{9J} could reproduce the J dependence in both the microwave and beam data, whereas the fit with F_{6J} could reproduce only the microwave portion. If F_{6J} is used rather than F_{9J} the main changes are small decreases in the magnitude of four parameters: 309 kHz in B and A, 52 kHz in D_{Jm}, and 3.3 MHz in F_{3J}. If both F_{6J} and F_{9J} are included in the fit, the two are equal to within their errors of ~50% and the χ^2 improves only marginally.

In an attempt to determine the true values of A and V_3 from the effective ones, two additional fits were made, one with $F_{3K} \equiv 0$ and the other with $D_{Km} \equiv 0$. The results are given in Table V. Although the magnitudes obtained for D_{Km} and F_{3K} appear large at first glance compared to those for D_{Jm} and F_{3J}, respectively, it must be remembered that $D_K/D_J = 18$. There appear to be no grounds for eliminating either D_{Km} or F_{3K}. The actual values for A and V_3 will most likely lie between the limiting numbers from Table V. As our final results, we take $A = 56179\ (75)$ MHz and $V_3 = 592.2\ (1.0)\ cm^{-1}$. These correlation effects have now been removed from this value of V_3 so that it is the "true" value in the context of a model where $V_{3n} \equiv 0$ for $n > 1$. However, this value still contains the usual contributions (*2*) from these higher-order terms in the expansion of the potential.

In the analysis, Hirota's data with $v = 3$ and 4 were deliberately omitted. The model cannot be made to fit these frequencies. The difficulty does not seem to be in the measurements or the identification, but appears to be in the model itself.

A detailed comparison between the constants obtained here and those determined in earlier works on methyl silane (*3*, *8*, *9*) is of very limited value and so is not presented here. With only the microwave data available, the earlier authors could not establish the difficulty with the lines with $v > 2$ and so included them in their analyses. Furthermore, F and ρ had to be calculated from the structure. Within these limitations, the earlier results are in reasonable agreement with the present values.

However, it is of interest to compare the current determination of I_α with the values obtained for asymmetric rotors using microwave spectroscopy. From Eq. (3), I_α for $CH_3{}^{28}SiH_3$ = 3.165 (5) amu-Å^2. A typical selection of results for asymmetric tops is given in Table V of Ref. (*19*). The present measurement falls in the middle of the range given and the accuracies are comparable.

The data for the isotopic species $CH_3{}^{30}SiH_3$ in Table III were analyzed in a manner similar to that used for $CH_3{}^{28}SiH_3$. The rotational constant B was set equal to the mm-wave value (*10*) and all the distortion constants were held fixed at the corresponding values for the parent isotopic species. Then the three remaining constants A^{eff}, V^{eff}, and ρ were varied. The results of the least-squares fit are given in Table IV.

The isotopic changes in A and V_3 can be taken directly from the differences in the effective values (see Eq. 16) because the distortion constants D_{Km} and F_{3K} can be assumed to cancel. The fractional change in A is

$$[A(CH_3{}^{30}SiH_3)/A(CH_3{}^{28}SiH_3) - 1] = 15(2) \text{ ppm.} \tag{17}$$

As expected for the on-axis substitution of a heavy atom, this shift is very small. It is probably due to changes in the zero point motion. The change in V_3 is

$$[V_3(CH_3{}^{30}SiH_3) - V_3(CH_3{}^{28}SiH_3)] = 0.106(11) \text{ cm}^{-1}. \tag{18}$$

The magnitude of the fractional change is ~180 ppm. Since this is the first measurement of its kind in a symmetric rotor, the order of magnitude is difficult to interpret.

The isotopic change in ρ can best be determined by using the relative (J = 1) measurements made for $[\nu_{EE}(30) - \nu_{EE}(28)]$ and $[\nu_{EA}(30) - \nu_{EA}(28)]$ as given in Table III. This gives a fractional change of

$$[\rho(CH_3{}^{30}SiH_3)/\rho(CH_3{}^{28}SiH_3) - 1] = 20(20) \text{ ppm.} \tag{19}$$

Equations (17) and (19) can be used to show that

$$[I_\alpha(CH_3{}^{30}SiH_3)/I_\alpha(CH_3{}^{28}SiH_3) - 1] = 5(20) \text{ ppm.} \tag{20}$$

As expected, the moment of inertia of the top is very insensitive to the on-axis isotopic substitution in the frame.

The isotopic changes given in Eqs. (17) to (19) are insensitive to the particular choice of higher order parameters used in the fits generating Table IV. Furthermore, the effects due to A, V_3, and ρ are so much larger than those due to the distortion constants that we can neglect the errors introduced by assuming these constants are unchanged by the isotopic substitution.

In a later paper (*10*), extensive new microwave data will be presented along with an evaluation of the model for the torsion–rotation Hamiltonian. A more complete discussion will be given of several points touched on here, including the deviations in the microwave lines for $v \geq 3$, the information obtained on the higher-order terms in the potential, and the interpretation of the various constants.

ACKNOWLEDGMENTS

The authors would like to thank Dr. M. Wong and Dr. A. Dymanus for many fruitful discussions and Mr. F. A. van Rijn for his technical assistance. One of us (I.O.) wishes to express his appreciation to the Natural Sciences and Engineering Research Council of Canada for its support. Both authors would like to thank the North Atlantic Treaty Organization Research Grant Program for its support through Travel grant No. 1454.

RECEIVED: December 8, 1981

REFERENCES

1. W. GORDY AND R. L. COOK, "Microwave Molecular Spectra," Interscience, New York, 1970.
2. C. C. LIN AND J. D. SWALEN, *Rev. Mod. Phys.* **31,** 841–892 (1959).
3. D. KIVELSON, *J. Chem. Phys.* **22,** 1733–1739 (1954); **23,** 2230–2235 (1955); **27,** 980 (1957).
4. W. L. MEERTS AND I. OZIER, *Phys. Rev. Lett.* **41,** 1109–1112 (1978).
5. I. OZIER AND W. L. MEERTS, *Phys. Rev. Lett.* **40,** 226–229 (1978).
6. I. OZIER AND W. L. MEERTS, *Canad. J. Phys.* **59,** 150–172 (1981).
7. W. L. MEERTS AND I. OZIER, *J. Chem. Phys.* **75,** 596–603 (1981).
8. E. HIROTA, *J. Mol. Spectrosc.* **43,** 36–64 (1972).
9. C. S. EWIG, W. E. PALKE, AND B. KIRTMAN, *J. Chem. Phys.* **60,** 2749–2758 (1974).
10. M. WONG, I. OZIER, AND W. L. MEERTS, in preparation.
11. I. OZIER AND W. L. MEERTS, *J. Mol. Spectrosc.* **93,** 164–178 (1982).
12. B. KIRTMAN, *J. Chem. Phys.* **37,** 2516–2539 (1962).
13. P. R. BUNKER, *Mol. Phys.* **9,** 257–264 (1965).
14. F. H. DE LEEUW AND A. DYMANUS, *J. Mol. Spectrosc.* **48,** 427–445 (1973); F. H. DE LEEUW, Ph.D. thesis, Katholieke Universiteit, Nijmegen, The Netherlands, 1971.
15. H. DIJKERMAN, W. FLEGEL, G. GRÄFF, AND B. MÖNTER, *Z. Naturforsch A.* **27,** 100–110 (1972).
16. W. L. MEERTS AND I. OZIER, VIth International Seminar on High Resolution Infrared Spectroscopy, Liblice, Czechoslovakia, September, 1980.
17. G. H. FULLER, *J. Phys. Chem. Ref. Data* **5,** 835–1121 (1976).
18. E. A. CLARK AND A. WEBER, *J. Chem. Phys.* **45,** 1759–1766 (1966).
19. J. DEMAISON, D. SCHWOCH, B. T. TAN, AND H. D. RUDOLPH, *J. Mol. Spectrosc.* **83,** 391–400 (1980).